ISSN 0036-0236, Russian Journal of Inorganic Chemistry, 2020, Vol. 65, No. 11, pp. 1654–1661. © Pleiades Publishing, Ltd., 2020.
Russian Text © The Author(s), 2020, published in Zhurnal Neorganicheskoi Khimii, 2020, Vol. 65, No. 11, pp. 1461–1468.

SYNTHESIS AND PROPERTIES OF INORGANIC COMPOUNDS

Effects of Substitutions of Titanium(IV) Ions by Iron(III) and Niobium(V) Ions on Phase Formation in Lanthanide-Containing Systems Comprising Layered Bismuth Titanate Ferrite

A. V. Mitrofanova[a], *, E. A. Fortal'nova[a], M. G. Safronenko[a], E. D. Politova[b], A. V. Mosunov[c], and N. U. Venskovskii[a]

[a] *Russian University of Peoples Friendship, Moscow, 117198 Russia*
[b] *Semenov Federal Research Center for Chemical Physics, Moscow, 119991 Russia*
[c] *Moscow State University, Moscow, 119991 Russia*
**e-mail: chemistann@gmail.com*

Received April 17, 2020; revised June 16, 2020; accepted June 27, 2020

Abstract—Phase formation in the series of $Bi_3Nd_2Fe_{1+y}Ti_{3-2y}Nb_yO_{15}$ and $Bi_3Tb_2Fe_{1+y}Ti_{3-2y}Nb_yO_{15}$ (y = 0.0–0.6 and $\Delta y = 0.2$) samples is studied. When $Bi_3Nd_2Fe_{1+y}Ti_{3-2y}Nb_yO_{15}$ solid solutions (ss) are doped with niobium(V) ions, the formation of $Bi_3Nd_2FeTi_3O_{15}$ layered perovskite, a member of the Aurivillius phase family of general formula $A_{m-1}Bi_2B_mO_{3m+3}$ ($m = 4$), is not dominant in samples where $y \geq 0.2$. $Bi_4Ti_3O_{12}$ ($m = 3$) and $NdFeO_3$ phases are formed in the course of phase interaction under the chosen conditions. With higher niobium(V) amounts, a $Bi_2Ti_2O_7$-base pyrochlore ss phase is formed in the $Bi_3Tb_2Fe_{1+y}Ti_{3-2y}Nb_yO_{15}$ multicomponent system. Dielectric spectroscopy shows that the phases in samples of both series where $y > 0.0$ undergo structural alterations associated with magnetic and electric ordering.

Keywords: phase formation, Aurivillius phase, layered perovskite, pyrochlore structure, phase transitions
DOI: 10.1134/S0036023620110133

INTRODUCTION

Aurivillius phases having the general formula $A_{m-1}Bi_2B_mO_{3m+3}$ are structurally built of alternating charged layers $(Bi_2O_2)^{2+}$ and perovskite-like blocks built of m $(A_{m-1}B_mO_{3m+1})^{2-}$ layers [1]. Positions A can be occupied by Na^+, K^+, Ca^{2+}, Sr^{2+}, Ba^{2+}, Pb^{2+}, Bi^{3+}, and Ln^{3+} ions; positions B inside oxygen octahedra can be occupied by Ti^{4+}, Cr^{3+}, Ga^{3+}, Mn^{4+}, Fe^{3+}, Co^{3+}, Ni^{3+}, Nb^{5+}, Ta^{5+}, and W^{6+} ions [2].

$Bi_5FeTi_3O_{15}$, an Aurivillius phase with $m = 4$, has repeatedly attracted the attention of scientists and has been studied comprehensively [3–10]. At the Curie temperature T_C = 740°C, $Bi_5FeTi_3O_{15}$ experiences transition from the ferroelectric phase (orthorhombic space group $A2_1am$) to the paraelectric phase (tetragonal space group $I4/mmm$) [9, 11].

The properties of $Bi_5FeTi_3O_{15}$ can be modified by modifying its composition. Ion substitutions in the bismuth(III) and titanium(IV) positions in the $Bi_5FeTi_3O_{15}$ structure enable one to multiply expand the Aurivillius phase family [1, 12–22]; substitutions appreciably affect the electrophysical characteristics and thermal stability of ceramics [21]. These properties are important for layered perovskite-like structures to be used in advanced electronic industry. In addition, the Curie temperature can vary widely, decreasing or increasing depending on the nature and amount of the substituent ion (Table 1). Therefore, the study of such substitutions in the structure of Aurivillius phases is important for materials design for various technical applications, such as sensors, filters, resonators, multilayer capacitors, and memory devices.

In particular, Aurivillius phases are a promising class of compounds in the context of search for new multiferroics, i.e., phases having ferroelectric and magnetic properties [3]. The main task in this area is to increase the content of magnetic ions to accomplish stable long-range magnetic order at high temperatures. The Aurivillius phase family provides sufficient chemical flexibility and stability to manufacture and explore new formulations that are promising in this regard.

EXPERIMENTAL

Choosing the subject matters for our study of double ion substitutions in the $Bi_5FeTi_3O_{15}$ structure, we were guided by the results of studies into heterovalent ion substitutions in $Bi_5Fe_{1+y}Ti_{3-2y}Nb_yO_{15}$ or $Bi_5FeTi_{3-2y}[Fe_yNb_y]O_{15}$ [23]: $Bi_3Nd_2Fe_{1+y}Ti_{3-2y}Nb_yO_{15}$

Table 1. Ion substitutions in the bismuth(III) and titanium(IV) sublattices in the $Bi_5FeTi_3O_{15}$ structure

Ion	Compound	Unite cell parameters			T_C, °C	T_N, °C	Source
		a, Å	b, Å	c, Å			
–	$Bi_5FeTi_3O_{15}$	5.47722(6)	5.44365(6)	41.17004(37)	740	–193	[9, 10, 30]
Nd^{3+}	$Bi_4NdFeTi_3O_{15}$	5.4266	5.4106	41.2626	502	–216.7	[25]
Nd^{3+}, Gd^{3+}	$Bi_4Nd_{0.5}Gd_{0.5}FeTi_3O_{15}$	5.4218(6)	5.4175(6)	41.211(1)	240	–73	[16]
W^{6+}, Cr^{3+}	$Bi_5FeTi_{3-3x}(WCr_2)_xO_{15}$ $x = 0.0$–0.15	Orthorhombic crystal system			740–703	–	[20]
Gd^{3+}, Co^{3+}	$Bi_{4.25}Gd_{0.75}Fe_{0.5}Co_{0.5}Ti_3O_{15}$	5.4291	5.4095	41.3689	815	97	[19]

(BNdFTNb) and $Bi_3Tb_2Fe_{1+y}Ti_{3-2y}Nb_yO_{15}$ (BTbFTNb) solid solutions (ss), where $y = 0.0$–0.6 and $\Delta y = 0.2$.

BNdFTNb and BTbFTNb samples were prepared using muffle heat treatment by routine ceramic technology from bismuth(III), iron(III), titanium(IV), niobium(V), neodymium(III), and terbium (III,IV) oxides (all chemicals were of reagent grade) taken in stoichiometric proportions according to the tailored composition. Mixtures of precursor oxides were triturated with ethanol and pelletized at each heat-treatment step.

To study the processes that occur in BNdFTNb and BTbFTNb samples where $y = 0.0$–0.6 and $\Delta y = 0.2$, we chose the following schedule: $T_1 = 800$°C (6 h), $T_2 = 900$°C (6 h), $T_3 = 900$°C (6 h), and $T_4 = 1000$°C (3 h).

The phase composition of BNdFTNb and BTbFTNb was studied by X-ray powder diffraction on DRON-3 and DRON-7 diffractometers (λCuK_α = 1.54056 Å); unit cell parameters were refined using standard software. Differential thermal analysis and thermogravimetric analysis (DTA/TG: SDT Q-600, $\Delta T = 20$–1100°C, $v = 10$ deg/min) were used to study interactions of components in the stoichiometric batches. IR spectroscopy (Nicolet 6700, 4000–400 cm^{-1}, attenuated total reflection (Pike technology), diamond) was used to verify XRD data. The electrophysical properties of samples were studied by dielectric spectroscopy (HP 4284A, $\Delta T = 25$–1000°C (300–1200 K), $f = 100$ Hz–1 MHz (1 V), and Ag electrodes).

RESULTS AND DISCUSSION

DTA/TG of Stoichiometric Precursor Batches

In order to determine the synthesis parameters we considered related literature [15, 17, 18, 20, 21] and carried out DTA of stoichiometric precursor batches (Figs. 1a, 1b).

The thermal curves for BNdFTNb samples feature two endotherms without weight loss, one relating to the polymorphic transition in unreacted bismuth oxide, α-$Bi_2O_3 \rightarrow \delta$-$Bi_2O_3$ (~720°C), and the other to ferroelectric transition in newly formed bismuth ferrite $BiFeO_3$ ($T_C = 810$°C) (Fig. 1a) [24].

The DTA curves for the BTbFTNb series feature three endotherms. Two of them (at ~550 and 800°C) relate to removal of oxygen upon thermal decomposition of Tb_4O_7; the third one (at ~720°C), which is not accompanied with weight loss, as in BNdFTNb samples, characterizes the polymorphic transition α-$Bi_2O_3 \rightarrow \delta$-$Bi_2O_3$ (Fig. 1b).

The interaction of the components in the batches of both systems begins at temperatures below 800°C and is multistage [10].

X-ray Powder Diffraction Analysis

Phase analysis shows that samples in the BNdFTNb series after the first two steps of synthesis are multiphase and comprise similar sets of phases, namely, $Bi_4Ti_3O_{12}$, $Bi_5FeTi_3O_{15}$, $Bi_3Nd_5O_{12}$, $Bi_2Fe_4O_9$, and $NdFeO_3$, dominated by ss based on layered perovskite-like structures of Aurivillius phases: $Bi_5FeTi_3O_{15}$ ($m = 4$) and $Bi_4Ti_3O_{12}$ ($m = 3$) (Fig. 2).

As to longer anneals at $T = 900$°C, not only do they reduce the number of phases in BNdFTNb samples, but they also lead to the disappearance of the $Bi_5FeTi_3O_{15}$ phase in $y = 0.4$–0.6 samples. $Bi_4Ti_3O_{12}$- and $NdFeO_3$-base ss are formed in niobium-containing samples in the course of phase formation.

A rise in heat-treatment temperature to 1000°C has no effects on the phase composition of the BNdFTNb samples where $y = 0.2$–0.6 compared to the preceding step; in the $y = 0.0$ sample, phase formation ends with the formation of $Bi_5FeTi_3O_{15}$-base layered perovskite ss (Fig. 2).

All BTbFTNb samples after the first annealing step are also multiphase as shown by XRD. The set of their phases is the same for the entire range of $0.0 \le y \le 0.6$: $BiTbO_3$, Tb_2TiO_5, and $Bi_5FeTi_3O_{15}$. The strongest reflections in the X-ray diffraction patterns of these samples relate to $BiTbO_3$-base ss.

As the annealing temperature rises to $T_2 = 900$°C, an impurity pyrochlore-type phase $Bi_2Ti_2O_7$ appears

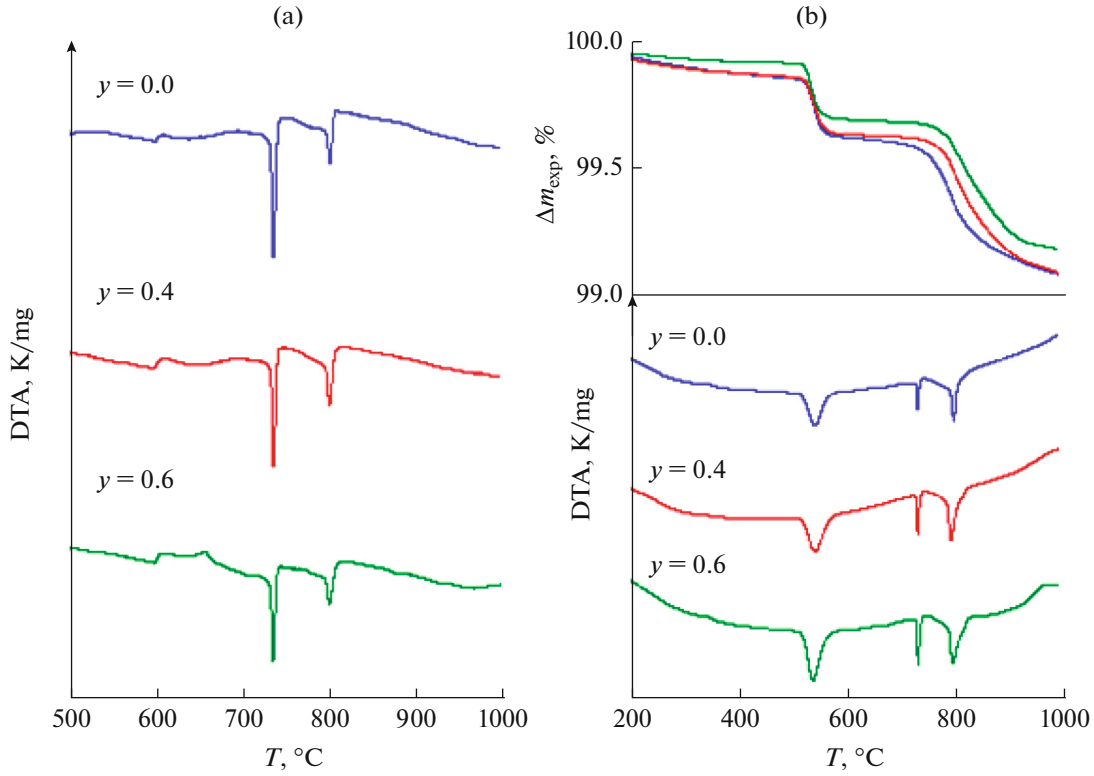

Fig. 1. Thermoanalytical curves for stoichiometric batches: (a) DTA curves for BNdFTNb samples and (b) DTA and TG curves for BTbFTNb samples.

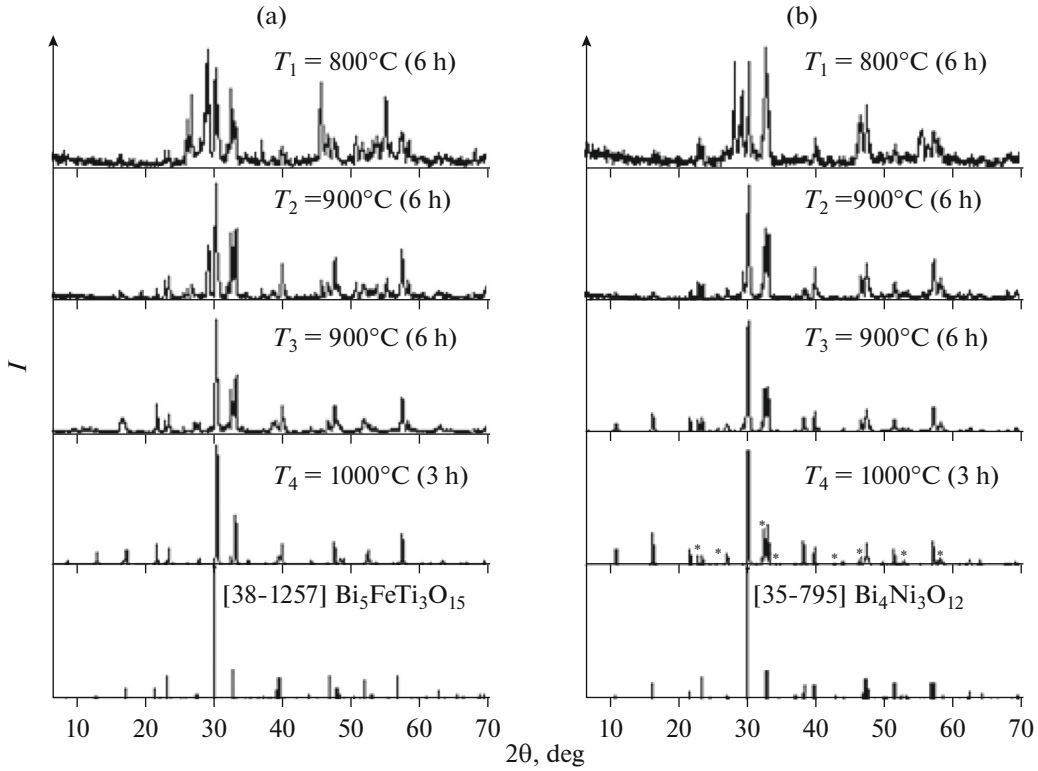

Fig. 2. X-ray phase diffraction patterns for BNdFTNb samples with y = (a) 0.0 and (b) 0.6; the $NdFeO_3$ phase is marked with an asterisk.

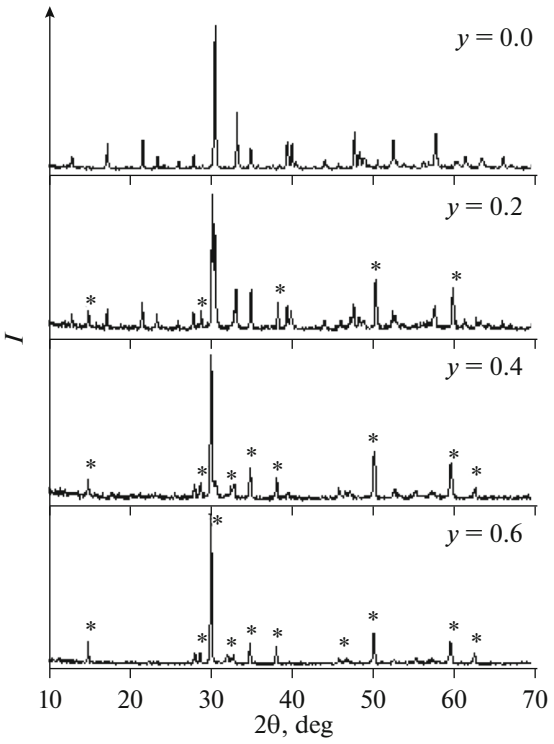

Fig. 3. X-ray phase diffraction patterns for BNdFTNb samples after annealing at T_4 = 1000°C (3 h); the $Bi_2Ti_2O_7$ phase is marked with an asterisk.

in all BTbFTNb batches, and the reflections from the $Bi_5FeTi_3O_{15}$ layered perovskite phase appreciably grow in intensity.

As the annealing time at 900°C increases (T_3, 6 h), $Bi_5FeTi_3O_{15}$-base ss phase formation is complete in the BTbFTNb end-member sample where y = 0.0, and the samples where $0.2 \le y \le 0.6$ comprise the $Bi_5FeTi_3O_{15}$ layered perovskite phase and $Bi_2Ti_2O_7$ pyrochlore phase coexisting in various proportions.

A further rise in annealing temperature to T_4 = 1000°C makes the samples denser, but does not affect the phase composition of BTbFTNb (Fig. 3). The reflections of the phases in X-ray diffraction patterns change their intensity ratio, which is an indirect evidence for a change in quantitative ratio of these phases. The y = 0.0 end-member remains a single phase. In the y = 0.2 sample the reflections of the $Bi_5FeTi_3O_{15}$ layered perovskite and $Bi_2Ti_2O_7$ pyrochlore have nearly equal intensities. In the y = 0.4 and 0.6 samples, the $Bi_2Ti_2O_7$-base phase has stronger reflections, and the $Bi_5FeTi_3O_{15}$-base phase decreases, as y rises, to trace amounts. The formation of the $Bi_2Ti_2O_7$-base pyrochlore phase in the studied BTb-FTNb series, this phase having an extensive homogeneity range, can be due to a deficit of bismuth(III) ions arising from their loss during high-temperature annealing [18, 25, 26].

An analysis of XRD data for the prepared BTbFTNb samples shows that the $Bi_5FeTi_3O_{15}$-base layered perovskite ss phase has an orthorhombically distorted unit cell and the $Bi_2Ti_2O_7$-base pyrochlore phase has a cubic structure (Table 2). The unit cell volume of the $Bi_3Tb_2FeTi_3O_{15}$ ss in the y = 0.0 sample is smaller than in unsubstituted $Bi_5FeTi_3O_{15}$, due to the substitution of ions in the Bi^{3+} sublattice by smaller Tb^{3+} ions (1.17 against 1.04 Å for CN = 8, respectively) [27] (Tables 1, 2). In the progress of doping of BTbFTNb samples where $0.2 \le y \le 0.6$ with Fe^{3+} and Nb^{5+} ions, which have a greater mean ionic radius than the Ti^{4+} ionic radius (0.64 against 0.605 Å for CN = 6, respectively) [27], the unit cell parameters increase linearly as y increases, in both the perovskite phase and the pyrochlore phase (Table 2). The elucidated trend, as well as the nonappearance of X-ray diffraction reflections from individual niobium-containing phases, points to the formation of $Bi_5FeTi_3O_{15}$- and $Bi_2Ti_2O_7$-base ss, where these ions are in the titanium(IV) sublattice.

IR Spectroscopy

The data derived from the IR spectra of samples of the BNdFTNb and BTbFTNb series are in agreement with the XRD results (Figs. 4a, 4b). In the BNdFTNb series, the $y \ge 0.2$ samples have identical set of phases comprised of $Bi_5FeTi_3O_{15}$-, $Bi_4Ti_3O_{12}$-, and $NdFeO_3$-base perovskite-like ss, whose IR spectra typically feature absorption bands in the ranges ~900–800 and ~700–500 cm^{-1} due to the M–O stretching vibrations in BO_6 octahedra of perovskite blocks (Fig. 4a). The

Table 2. Concentration-dependent unit cell parameters of the phases found in BtbFtNb samples as-annealed at T_4 = 1000°C (3 h)

y	$Bi_5FeTi_3O_{15}$-base phase				$Bi_2Ti_2O_7$-base phase	
	a, Å	b, Å	c, Å	V, Å^3	a, Å	V, Å^3
0.0	5.349(6)	5.415(7)	40.98(3)	1187(4)	–	–
0.2	5.382(5)	5.470(6)	41.03(3)	1208(3)	20.449(5)	8551(6)
0.4	5.401(4)	5.503(4)	41.05(3)	1220(2)	20.476(5)	8585(6)
0.6	–	–	–	–	20.585(5)	8723(6)

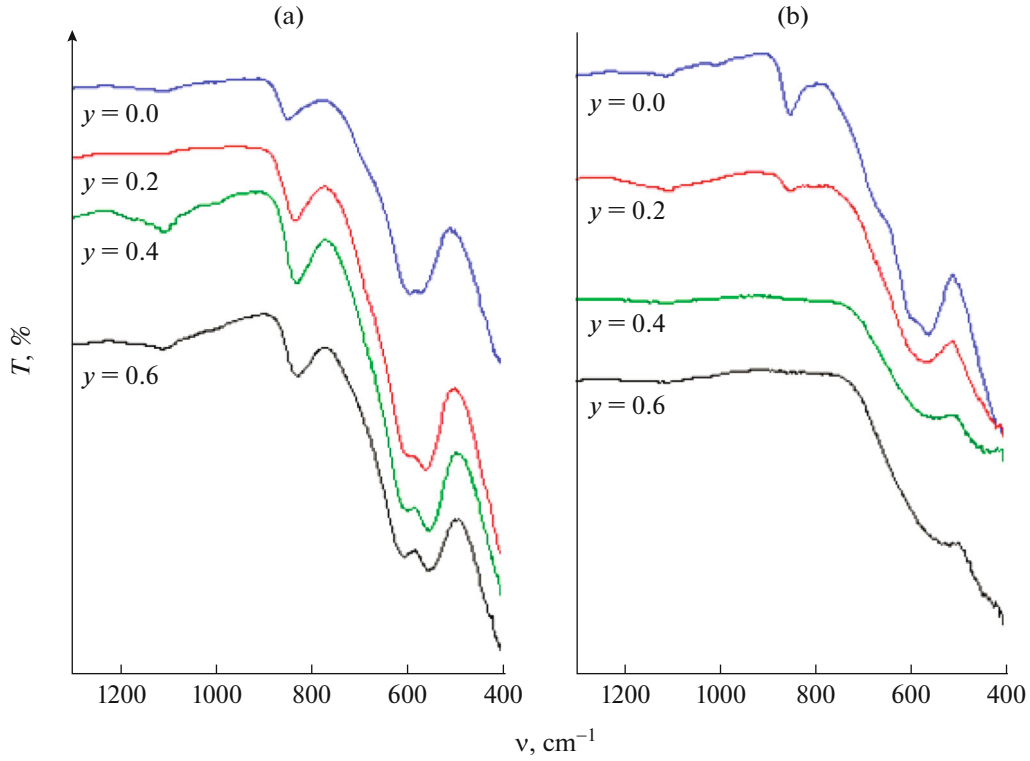

Fig. 4. IR spectra of (a) BNdFTNb and (b) BTbFTNb samples after annealing at T_4 = 1000°C (3 h).

split of the ~700–500 cm^{-1} absorption band strengthening in response to rising y is likely due to the changing quantitative phase ratio in the samples: the disappearance of the $Bi_5FeTi_3O_{15}$-base phase and the increase in amounts of the $NdFeO_3$-base perovskite phase.

The IR spectra of the BTbFTNb samples where $y = 0.0$ and 0.2, which are dominated by the $Bi_5FeTi_3O_{15}$-base perovskite phase as probed by XRD, also feature absorption bands typical of stretching vibrations in BO_6 octahedra, in the ranges ~900–800 and ~700–500 cm^{-1}. The evolution of the general spectral pattern in BTbFTNb samples in response to rising y and, accordingly, increasing amount of the $Bi_2Ti_2O_7$-base phase verifies the XRD observation of the formation of a pyrochlore-type phase in these samples [28].

Dielectric Spectroscopy

The dielectric-spectroscopic study of the electrophysical properties of the BNdFTNb and BTbFTNb samples as annealed at T_4 = 1000°C shows that, regardless of phase composition, all samples experience relaxation processes accompanied with frequency-dependent peaks on the dielectric permittivity curves (Figs. 5b, 6b). With this, the conductivity (σ) curves $\log\sigma(1000/T)$ feature frequency dispersion in the range ~298–500 K, typical of ionic conductivity (Figs. 5a, 6a) [1]. These observations imply that the phases have oxygen conductivity; that is, an anion-deficient oxygen sublattice is formed. The formation of this sublattice is due to the loss of bismuth in the course of high-temperature synthesis [18, 25, 26].

The second type of anomaly appears on the temperature-dependent dielectric permittivity curves ε(T) in the $y \geq 0.2$ samples of the BNdFTNb and BTbFTNb series at ~247–287°C (~520–560 K) and ~727°C (~1000 K), respectively, and these anomalies are independent of the electric field frequency (Figs. 5b, 6b). These anomalies are associated with changes in the crystal structure of the phases that make up the samples. They are not manifested in the BNdFTNb and BTbFTNb samples where y = 0.0, which are $Bi_3Nd_2FeTi_3O_{15}$ ss and $Bi_3Tb_2FeTi_3O_{15}$ ss, respectively. This implies that electric ordering in the $Bi_5FeTi_3O_{15}$ structure is inhibited upon an about 40 at % substitution of Bi(III) ions by Nd(III) and Tb(III) ions [29] (Table 1).

In the BNdFTNb series, the anomalies at ~247–287°C (~520–560 K) are due to the presence of a neodymium ferrite $NdFeO_3$ base phase, which undergoes antiferromagnetic-to-paramagnetic phase transition in this temperature range (T_N = 301°C/574 K) [30]. The temperature of this transition increasing in response to rise in y in BNdFTNb samples can be both due to the entrance of niobium(V) ions into the phase and due to a deficit in the ionic sublattice arising from the loss of bismuth(III) during high-temperature annealing

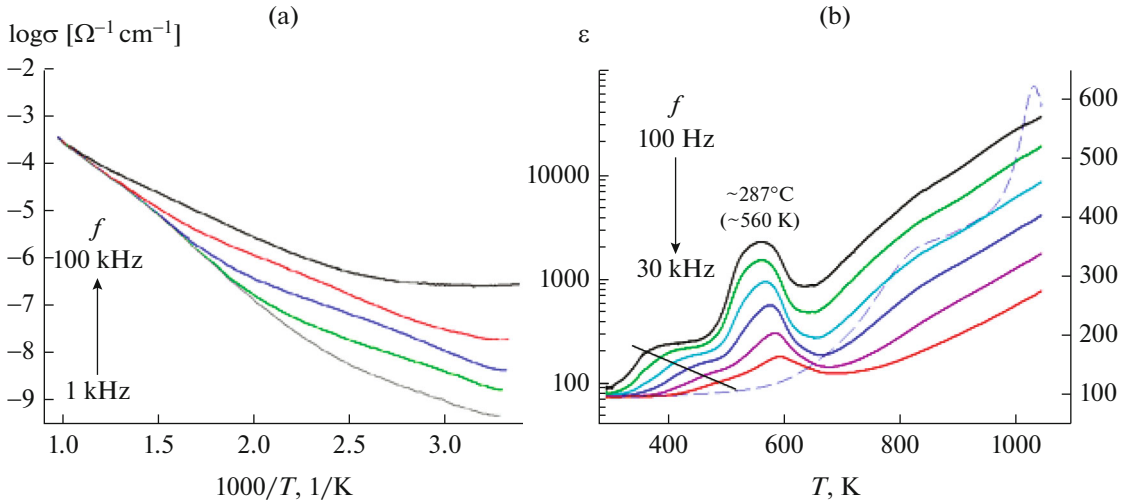

Fig. 5. (a) $\log\sigma(1000/T)$ plot for a BNdFTNb sample with $y = 0.0$ and (b) $\varepsilon(T)$ plot for a BNdFTNb sample with $y = 0.6$ after annealing at $T_4 = 1000$°C; the dashed curve is $\varepsilon(T)$ for $Bi_5FeTi_3O_{15}$ ($f = 30$ kHz).

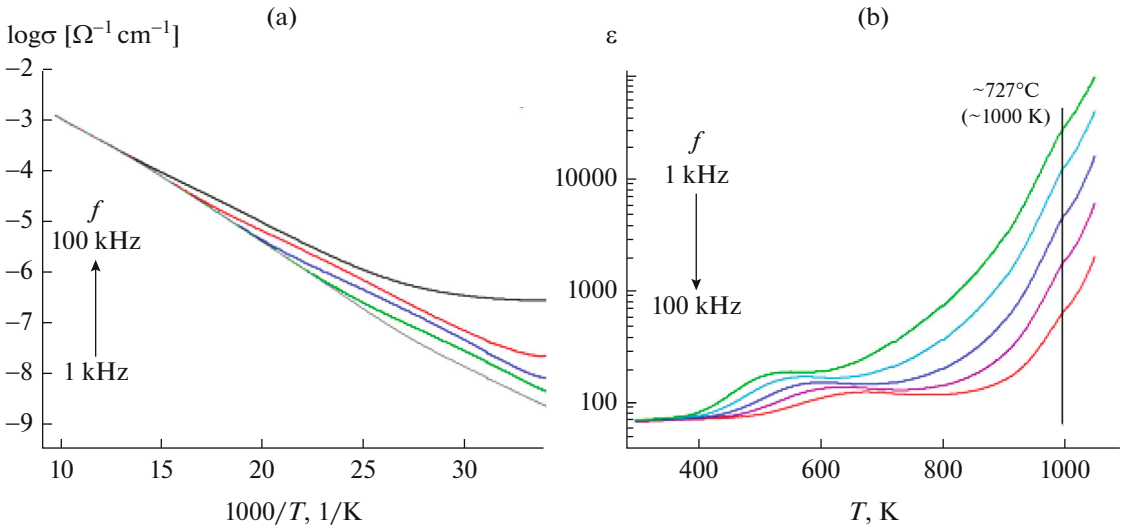

Fig. 6. (a) $\log\sigma(1000/T)$ plot for a BTbFTNb sample with $y = 0.0$ and (b) $\varepsilon(T)$ plot for a BTbFTNb sample with $y = 0.6$ after annealing at $T_4 = 1000$°C.

[31]. Similar reasons can stand behind the absence of $\varepsilon(T)$ anomalies associated with electric disordering in the $Bi_4Ti_3O_{12}$ phase (T_C = ~675°C/~948 K) [32].

In the $y \geq 0.2$ samples of the BTbFTNb series, unfortunately, it is difficult to exactly assign the frequency-independent $\varepsilon(T)$ anomalies. These samples as probed by XRD comprise the $Bi_5FeTi_3O_{15}$-base phase (T_C = 740°C/1013 K) [9, 11, 33] and $Bi_2Ti_2O_7$-base phase; the pyrochlore structure of the latter can experience order–disorder transitions both at ~1000°C/~1273 K and at higher temperatures [34, 35]. In addition, all of the detected phases are solid solutions containing Nd(III), Tb(III), Fe(III), and Nb(V) ions, and they can undergo alterations associated either with structural rearrangement or with release of electric ordering. Still further, Nb^{5+} ions, like Nd^{3+} and Tb^{3+}, too, have an appreciable effect on the temperatures of these transformations.

CONCLUSIONS

As a result of our study, we discovered that the incorporation of iron(III) and niobium(V) ions into the titanium(IV) sublattice of the $Bi_3Nd_2FeTi_3O_{15}$ structure gives rise to the formation of perovskite phases based on layered titanate $Bi_4Ti_3O_{12}$ ($m = 3$) and

ferrite $NdFeO_3$ in the $Bi_3Nd_2Fe_{1+y}Ti_{3-2y}Nb_yO_{15}$ (BNdFTNb) series. Higher amounts of these ions in $Bi_3Tb_2Fe_{1+y}Ti_{3-2y}Nb_yO_{15}$ (BTbFTNb) favor the formation of a $Bi_2Ti_2O_7$-base pyrochlore ss phase. Both the orthorhombic $Bi_5FeTi_3O_{15}$-base perovskite phase and the cubic pyrochlore phase have their unit cell parameters increasing, as y increases, due to partial substitutions of Ti^{4+} ions by Fe^{3+} and Nb^{5+} whose average ionic radius is greater.

We used dielectric spectroscopy to study the thermal behavior of BNdFTNb and BTbFTNb samples. These samples have been found to have oxygen conductivity; that is, they have an anion-deficient sublattice. This is due to the loss of bismuth(III) oxide in the course of high-temperature annealing. An about 40 at % substitution of bismuth ions by neodymium(III) and terbium(III) ions inhibits electronic ordering in BNdFTNb and BTbFTNb ss where $y = 0.0$. The $\varepsilon(T)$ temperature-dependent curves for samples of both series where $y > 0.0$ feature anomalies related to changes in the magnetic and electric structures of the detected phases.

FUNDING

The study was supported by the Semenov Federal Research Center for Chemical Physics of the Russian Academy of Sciences in part of the fulfillment of the Governmental task (theme No. 45.22 (AAAA-A18-118012390045-2)).

CONFLICT OF INTEREST

The authors have no conflicts of interests to declare.

REFERECNES

1. M. S. Shashkov, O. V. Malyshkina, I. V. Piir, and M. S. Koroleva, Phys. Solid State **57**, 518 (2015). https://doi.org/10.1134/S1063783415030312
2. V. G. Vlasenko, S. V. Zubkov, V. A. Shuvaeva, et al., Fiz. Tverd. Tela **56**, 15040 (2014).
3. A. Y. Birenbaum and C. Ederer, Phys. Rev. B **90**, 214109 (2014). https://doi.org/10.1103/PhysRevB.90.214109
4. X. Gao, L. Zhang, C. Wang, and Q. Shen, J. Eur. Ceram. Soc. **37**, 2399 (2017). https://doi.org/10.1016/j.jeurceramsoc.2017.01.037
5. M. Garcia-Guaderrama, G. G. Carbajal-Arizaga, and A. Duran, Ceram. Int. **40**, 7459 (2014). https://doi.org/10.1016/j.ceramint.2013.12.094
6. A. Lisinska-Czekaj, J. Plewa, and D. Czekaj, Cie. Technol. Mater. **29**, 210 (2017). https://doi.org/10.1016/j.ctmat.2016.04.006
7. T. Pikula, J. Dzik, P. Guzdek, et al., Ceram. Int. **43**, 11442 (2017). https://doi.org/10.1016/j.ceramint.2017.06.008
8. M. Wu, Zh. Tian, S. Yuan, and Zh. Huang, Mater. Lett. **68**, 190 (2012). https://doi.org/10.1016/j.matlet.2011.09.113
9. J.-J. Ji, H. Sun, X.-Y. Mao, et al., J. Sol-Gel Sci. Technol. **61**, 328 (2012). https://doi.org/10.1007/s10971-011-2631-4
10. N. A. Lomanova, M. I. Morozov, V. L. Ugolkov, and V. V. Gusarov, Neorg. Mater. **42**, 225 (2006).
11. J. D. Bobic, R. M. Katiliute, M. Ivanov, et al., J. Mater. Sci.: Mater. Electron. **27**, 2448 (2016). https://doi.org/10.1007/s10854-015-4044-6
12. Y. Bai, J. Chen, R. Tian, and S. Zhao, Mater. Lett. **164**, 618 (2016). https://doi.org/10.1016/j.matlet.2015.11.083
13. C.-X. Chen, Y.-K. Liu, and R.-K. Zheng, J. Mater. Sci.: Mater. Electron. **28**, 7562 (2017). https://doi.org/10.1007/s10854-017-6446-0
14. X. Chen, Z. Lu, F. Huang, et al., J. Alloys Compd. **693**, 448 (2017). https://doi.org/10.1016/j.jallcom.2016.09.214
15. X. Chen, J. Xiao, Y. Xue, et al., Ceram. Int. **40**, 2635 (2014). https://doi.org/10.1016/j.ceramint.2013.10.063
16. H. J. Kim, L. W. Kim, L. Y. Choi, et al., J. Korean Phys. Soc. **63**, 2330 (2013). https://doi.org/10.3938/jkps.63.2330
17. F. Rehman, H.-B. Jin, C. Niu, et al., Ceram. Int. **42**, 2806 (2016). https://doi.org/10.1016/j.ceramint.2015.11.013
18. R. Ti, F. Huang, W. Zhu, et al., Ceram. Int. **41**, 453 (2015). https://doi.org/10.1016/j.ceramint.2015.03.157
19. X. Z. Zuo, M. L. Zhang, E. J. He, et al., J. Alloys Compd. **695**, 2556 (2017). https://doi.org/10.1016/j.jallcom.2016.11.161
20. X. Zuo, M. Zhang, E. He, et al., J. Alloys Compd. **726**, 1040 (2017). https://doi.org/10.1016/j.jallcom.2017.08.077
21. Novoa O. D. Gil, Tellez D. A. Landínez, and J. Roa-Rojas, Rev. Mex. Fis. **58** (2), 77 (2012). https://doi.org/10.1016/j.physb.2011.12.035
22. N. A. Lomanova, V. L. Ugolkov, V. V. Panchuk, and V. G. Semenov, Russ. J. Gen. Chem. **87**, 365 (2017). https://doi.org/10.1134/S107036321703001X
23. A. V. Mitrofanova, E. A. Fortal'nova, M. G. Safronenko, et al., Nauch.-Tekh. Vestn. Povolzh., No. 3, 31 (2019).
24. J. Wang, J. B. Neaton, H. Zheng, et al., Science **299**, 1719 (2003). https://doi.org/10.1126/science.1080615
25. D. Zhang, L. Feng, W. Huang, et al., J. Appl. Phys. **120**, 154105 (2016). https://doi.org/10.1063/1.4965702
26. W. Bai, C. Chen, J. Yang, et al., Sci. Rep. **5**, 17846 (2015). https://doi.org/10.1038/srep17846
27. R. D. Shannon and C. T. Prewitt, Acta Crystallogr., Sect. B: Struct. Sci. **25**, 925 (1969). https://doi.org/10.1107/S0567740869003220
28. N. V. Gundobin, F. M. Spiridonov, L. N. Komissarova, and K. I. Petrov, Zh. Neorg. Khim. **20**, 582 (1975).
29. S. A. Ivanov, T. Sarkar, E. A. Fortalnova, et al., J. Mater. Sci.: Mater. Electron. **28**, 7692 (2017). https://doi.org/10.1007/s10854-017-6463-z

30. S. C. Parida, S. K. Rakshit, and Z. Singh, J. Solid State Chem. **181**, 101 (2008). https://doi.org/10.1016/j.jssc.2007.11.003

31. G. L. Yuan and S. W. Or, Appl. Phys. Lett. **88**, 062905 (2006).

32. Z. Peng, Q. Chen, Y. Chen, et al., Mater. Res. Bull. **59**, 125 (2014). https://doi.org/10.1016/j.materresbull.2014.07.002

33. E. Jartych, T. Pikula, M. Mazurek, et al., J. Magn. Magn. Mater. **342**, 27 (2013). https://doi.org/10.1016/j.jmmm.2013.04.046

34. Yu. V. Kabirov, M. F. Kupriyanov, and E. V. Chebanova, Zh. Strukt. Khim. **50**, 492 (2009).

35. K. W. Eberman, Solid State Ionics **148**, 521 (2002). https://doi.org/10.1016/S0167-2738(02)00099-1

Translated by O. Fedorova